IEEE Access
Multidisciplinary | Rapid Review | Open Access Journal

Received 16 October 2023, accepted 26 October 2023, date of publication 30 October 2023, date of current version 3 November 2023.

Digital Object Identifier 10.1109/ACCESS.2023.3328619

STANDARDS

Quality Assessment of Metal Additive Manufactured Parts by a Multiscale Convolutional Fuzzy Neural Network Using Ultrasound Images as Input Data

CHUN-HUI LIN[1], CHENG-JIAN LIN[2], (Senior Member, IEEE), AND SHYH-HAU WANG[1], (Senior Member, IEEE)

[1]Department of Computer Science and Information Engineering, National Cheng Kung University, Tainan 701, Taiwan
[2]Department of Computer Science and Information Engineering, National Chin-Yi University of Technology, Taichung 411, Taiwan

Corresponding author: Cheng-Jian Lin (cjlin@ncut.edu.tw)

This work was supported by the "Intelligent Manufacturing Research Center" (iMRC) from The Featured Areas Research Center Program within the framework of the Higher Education Sprout Project by the Ministry of Education (MOE) in Taiwan.

ABSTRACT The successful production of metallic workpieces through selective laser melting requires a quality assurance process that can effectively and nondestructively assess internal defects. Ultrasound testing is a nondestructive testing modality that can be used to identify defects and characterize the microstructure and properties of a material. Moreover, developments in computer vision techniques have led to the increased use of neural networks (NNs) in quality assurance processes. Therefore, a novel multiscale convolutional fuzzy NN (MCFNN) that uses ultrasound images as input data was developed in this study to automatically evaluate Inconel 718 workpieces fabricated through selective laser melting under various combinations of process parameters. The average accuracy, precision, recall, F1 score, and number of required parameters for the developed MCFNN were comparable to those of state-of-the-art models. Moreover, several concatenation methods, multiscale fusion strategies, and fuzzy inference systems were implemented in the developed MCFNN for performance comparison. Subsequently, the workpieces were examined through microcomputed tomography to verify the results obtained using ultrasound images. The experimental results indicated that among the compared models, the MCFNN achieved the highest average accuracy (91.44% $\pm$ 4.73%), precision (92.74% $\pm$ 3.79%), recall (91.44% $\pm$ 4.73%), and F1 score (91.35% $\pm$ 4.82%) and required the fewest parameters (107,138). The experimental results demonstrate that the developed MCFNN has high potential for implementation in the embedded devices of portable ultrasound scanning systems.

INDEX TERMS Automated quality assessment, fuzzy neural network, multiscale convolutional neural network, metal additive manufacturing, ultrasound testing.

I. INTRODUCTION

Metal additive manufacturing (AM) technologies have been widely applied in the aerospace, automotive, and medical fields, as well as other fields, because they enable rapid production and provide design freedom [1]. In particular, powder bed fusion (PBF) is a metal AM process that offers numerous benefits and is currently receiving increasing attention as an emerging polymer and metal AM technology [2]. Selective laser melting (SLM) is the most widely used PBF process [3] and can produce near-net-shaped parts with suitable mechanical properties, an appropriate surface finish appearance, and complex geometries. Because of the suitable mechanical properties and lightweight characteristics of materials fabricated through SLM, the demand for SLM has swiftly increased in recent years [4]; however, complex physical phenomena—such as heat transfer, molten metal flow, and phase transformation—strongly affect the final product quality in SLM [5]. To maintain a high-quality fabricated workpiece, properties of powder, process parameters, and

The associate editor coordinating the review of this manuscript and approving it for publication was Wuliang Yin.

© 2023 The Authors. This work is licensed under a Creative Commons Attribution-NonCommercial-NoDerivatives 4.0 License.
For more information, see https://creativecommons.org/licenses/by-nc-nd/4.0/

Technique	Porosity	Unfused powder	Cracks	Microstructural disturbance	Mechanical properties
Eddy Current Testing	✓	-	✓✓	×	×
Penetrant Testing	×	✓	✓	×	✓
Xray-Computed Tomography (CT)	✓✓	✓✓	✓✓	-	-
Ultrasonic Testing (UT)	✓✓	✓✓	✓✓	✓✓	✓✓

✓ ✓: applicable with high reliability, ✓: possible to apply but certain conditions required, × : not applicable to AM fault detection, -: not mentioned

FIGURE 1. Advantages of each NDT modality.

finite-element (FE) software construction must be considered before manufacturing [6]. Moreover, the effects of various process parameters on the manufacturing process should be understood so that these parameters can be optimized to improve the manufactured product. Liu et al. explored the tensile behavior and microhardness of SS 316L stainless-steel workpieces fabricated through SLM under various scanning speeds; their experimental results indicated that the scanning speed strongly influenced the melting pool boundaries, residual pores, solidification cells, nano-inclusions, grain size, and grain distributions of the workpieces [7]. The authors of [8] found that the quality of SLM workpieces such as the variations of structural anisotropy and heterogeneity texture depended on the process parameters adopted for manufacturing. In [9], the uniformity of the material properties and mechanical properties of workpieces could not be satisfactorily maintained under cyclic thermal loading. Therefore, quality assurance—including the assessment of voids, porosity, and undesirable grain characteristics—must be performed for metallic workpieces manufactured through SLM to ensure the success of their application [10].

Many nondestructive testing (NDT) techniques—such as eddy current testing, penetrant testing, X-ray computed tomography (CT), infrared thermographic testing, acoustic emission testing, and ultrasound testing (UT)—are feasible and practical for assessing metallic workpieces manufactured through SLM [11]. The advantages of each NDT modality are listed in Fig. 1. Specifically, UT is a highly flexible, rapid, and cost-effective method for detecting and evaluating surface, subsurface, and internal defects of objects [12]. The pulse-echo technique is frequently applied in UT to measure internal voids, cracks, and microstructures of metallic workpieces fabricated through SLM [13]. The components of the echo signals received from the ultrasound system can be analyzed to determine several properties, including the average grain diameter, microstructure orientation, and morphology of an object [14]. Kim et al. evaluated the defects and microstructural differences of AM SS316L stainless-steel workpieces fabricated under various parameters of the hatch spacing process by using ultrasound phase velocity measurements. Their results confirmed that phase velocity is sensitive to pore geometry and crystallographic texture [15]. Yuan and Yu measured the attenuation and velocity of ultrasonic elastic waves under various laser strengths by using the ultrasonic immersion technique. The velocity and attenuation results revealed that the laser power influenced workpiece microstructures oriented in different directions and the capability of inspecting internal defects [16]. Huang et al. investigated the attenuation of ultrasound waves and the relationship between their phase velocity and porosity in relation to multiple workpiece depths; they found that this attenuation and relationship were sensitive to grain size and porosity. In addition, the feasibility of using UT to detect variances in microstructural and mechanical properties was revealed in [17]. Nevertheless, using UT for the thorough quantitative analysis of the internal defects, microstructural orientation, and morphology of metallic workpieces manufactured through AM is a challenging task.

Fortunately, artificial intelligence methods, such as machine learning (ML) and deep learning (DL) [18], are useful for extracting implicit knowledge from a dataset; thus, these methods can be used to characterize in detail the internal properties of objects manufactured through SLM. Furthermore, these methods can be used to determine relationships among process parameters and the quality of products produced through SLM; yet some models require many training parameters. To reduce the computational costs of CNNs without drastically reducing their accuracy, numerous CNN compression techniques—including network pruning, parameter quantization, and low-rank decomposition—have been developed. Another method for reducing computational cost involves decreasing the number of parameters required in the fully connected layer of an CNN. In particular, fuzzy NNs (FNNs), which combine the strengths of NNs and fuzzy logic, have been applied to solve industrial classification, prediction, and control problems for more than 40 years [19]. The advantages of FNNs are their abilities to design fuzzy rules automatically and integrate numerical data with expert knowledge. Moreover, they search the parameters of a fuzzy system by exploiting the approximation techniques of NNs, which require relatively few training parameters. Some relevant studies on FNNs are described as follows. Campos Souza et al. designed an extreme learning machine–based algorithm for an FNN to solve binary pattern classification problems [20]. Khodabandelou and Ebadzadeh proposed a Takagi–Sugeno–Kang (TSK) FNN combined with a support

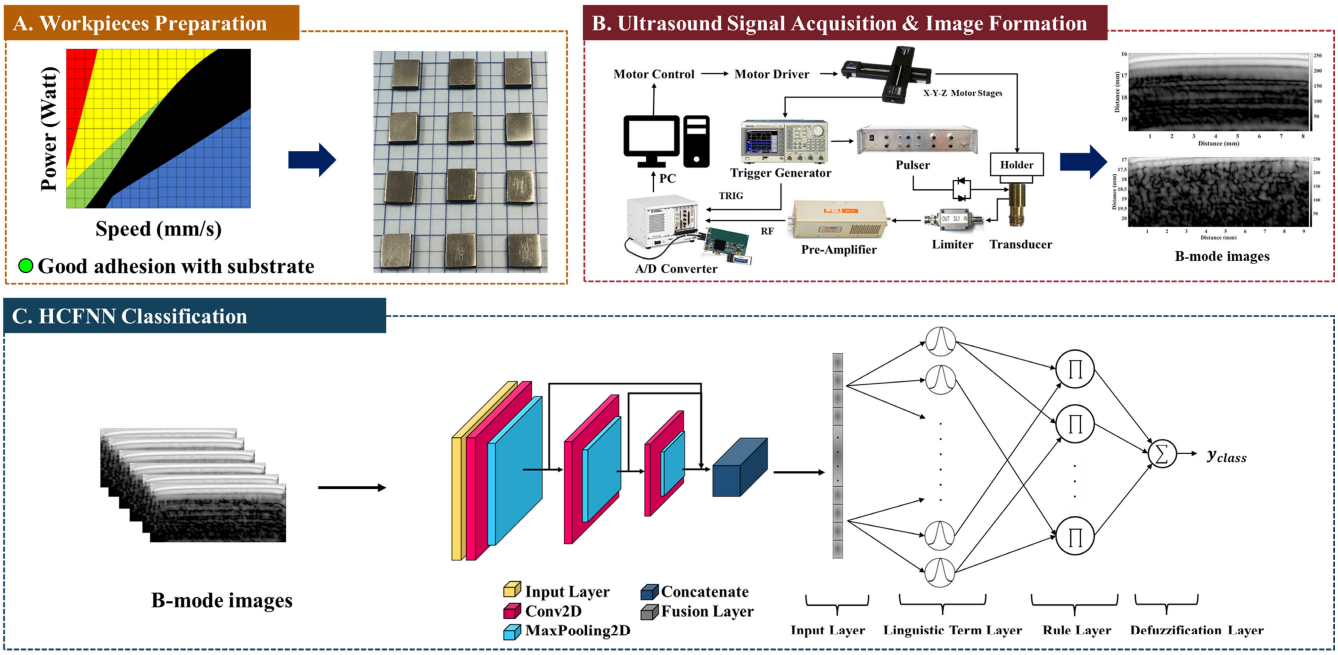

FIGURE 2. Workflow of the present study.

vector machine (SVM) model to leverage the relationship between an SVM kernel and an FNN. Their results indicated that this combined model outperformed conventional SVM and FNN models in classification tasks [21]. Overall, FNNs have low computational complexity, high interpretability, and high accuracy and can manage imprecise data when applied alongside ML algorithms.

Accordingly, in the present study, to maintain the image extraction ability of CNNs and the characteristics of FNNs, a multiscale convolutional FNN (MCFNN) was developed to automatically and accurately assess the quality of workpieces manufactured through AM. First, metallic workpieces were fabricated through SLM under various combinations of process parameters (e.g., laser power, scanning speed, and layer thickness) by using a commercial SLM machine. The combinations of process parameters were selected according to simulation results. The quality of the fabricated workpieces was measured using an analytical balance to divide the workpieces into two quality groups. Subsequently, ultrasound B-mode signals and images were acquired using a high-frequency ultrasound system. The proposed MCFNN model and state-of-the-art DL architectures were then used to classify the workpiece quality by using the acquired ultrasound images as input. Moreover, multiple multiscale fusion strategies and fuzzy inference systems were implemented in the designed MCFNN for performance comparison. Finally, the average accuracy, precision, recall, F1 score, and number of required parameters of the MCFNN were compared with those of the other models. To verify the workpiece quality, the fabricated workpieces were sent to the Metal Industries Research & Development Centre, Kaohsiung, Taiwan, for micro-CT scanning.

The contributions of this study are described as follows:

(1) A suitable UT scanning system was developed to characterize the internal defects and microstructural changes of metallic workpieces of varying quality that had been fabricated through SLM.
(2) The proposed MCFNN model can accurately classify the quality of metallic workpieces manufactured through SLM from ultrasound B-mode images.
(3) The proposed MCFNN exhibited higher average accuracy (91.44%), precision (92.74%), and recall (91.44%) and a higher F1 score (91.35%) as well as lower standard deviations compared with the other models. Moreover, the proposed model required fewer training parameters (107,138) in the quality classification task than did the other models.

The remainder of this paper is organized as follows: Section II provides a detailed description of the materials and methods used in this study, including the experimental arrangements for the fabrication of metallic workpieces through SLM, ultrasound signal and image acquisition, and the proposed MCFNN. Sections III and VI present the experimental results and a discussion related to these results, respectively. Finally, the conclusions of this study and recommendations for future research are provided in Section V.

II. MATERIALS AND METHODS

The developed MCFNN has the ability to extract image features and requires few training parameters. This network combines the advantages of CNNs and FNNs for the automatic and accurate assessment of the quality of metallic workpieces produced through SLM. The three parts of this study, namely 1) the fabrication of metallic workpieces

through SLM, 2) the acquisition of ultrasound signals and images, and 3) the construction of the proposed MCFNN model, are summarized in Fig. 2 and described in detail in this section.

A. PREPARATION OF METALLIC WORKPIECES THROUGH SLM

The heat input to the material powder directly affects thermal behaviors during SLM. The laser energy used in SLM can be expressed as laser energy density (LED), which is defined as the amount of laser energy delivered to a unit volume of powder material [22]. LED is expressed as follows:

$$Laser\ energy\ density\ (LED) = \frac{P}{v * s * t} \tag{1}$$

where P, v, s, and t denote laser power (W), scanning speed (mm/s), hatch space (mm), and layer thickness (mm), respectively. Different materials require different optimal process parameters, in this study, Inconel 718 metallic powder was selected for fabrication and the process parameter combinations were selected according to the simulations of Tran et al. [23]. Considering the properties of the adopted SLM machine (AMP-250, Tongtai, Kaohsiung City, Taiwan), 24 Inconel 718 workpieces with dimensions of 10 × 10 × 5 mm^3 each were fabricated under laser power, scanning speed, and layer thickness ranges of 200–300 W, 850–1000 mm/s, and 20–40 μm, respectively.

B. WORKPIECE POROSITY MEASUREMENT

After the manufacturing of the workpieces, their quality was measured using an analytical balance (AB54-S, Mettler Toledo, Greifensee, Switzerland) according to Archimedes' principle [24]. The fluid used in the present study was 95% ethanol. The porosity of the workpieces was calculated after determining their density. To classify workpiece quality, the workpieces were divided into two classes based on porosity. These classes served as the output labels for the proposed classification model: those with porosity of $\leq$1.5% and those with porosity of $>$1.5%.

C. ULTRASOUND SIGNAL AND IMAGE ACQUISITION

UT can reveal internal defects and microstructural variations within workpieces. Thus, ultrasound images constitute appropriate input data for DL models designed to detect workpiece quality. To acquire ultrasound images, a high-frequency ultrasound imaging system was developed in the present study, as depicted in Fig. 2 Part B. The actual photo of the experiment is presented in Fig. 3.

To achieve a suitable trade-off between penetration depth and image spatial resolution, an ultrasound transducer with a frequency of 20 MHz was used. The developed high-frequency ultrasound imaging system mainly comprised a 20-MHz, single-element ultrasound transducer (NIH Ultrasonic Transducer Resource Center, University of Southern California, Los Angeles, CA, USA), a pulser (AVB2-TB-C-EA-EF, AVTECH Electrosystems Ltd., Ottawa, Ontario, Canada), X–Y–Z motor stages (Model SGSP26-200, Sigma Koki, Tokyo, Japan), a motor controller (Model CSG-602R, Sigma Koki), and an 8-bit analog-to-digital converter (PXI-5152, National Instruments, Austin, TX, USA). A data acquisition system was synchronized with the X–Y–Z motor stages and controlled with a program developed using LabVIEW software (National Instruments, USA). The pulse-echo response of the transducer is displayed in Fig. 4, and the characteristics of the transducer are presented in Table 1.

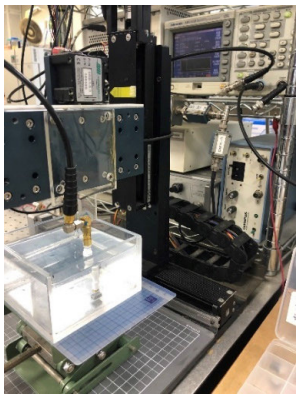

FIGURE 3. Actual photo of the experiment.

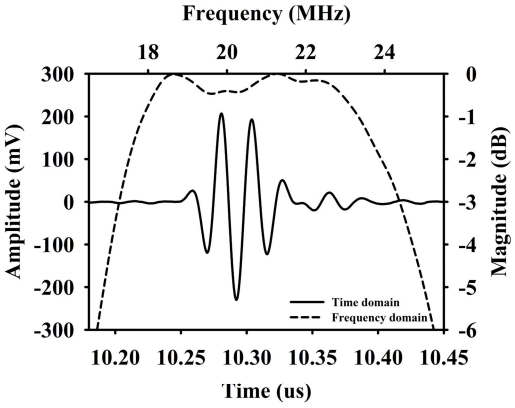

FIGURE 4. Workflow of the present study.

TABLE 1. Characteristics of the adopted transducer.

Center Frequency (MHz)	18.6
Aperture Size (mm)	6.5
f-number	2.4
-6dB Bandwidth (MHz)	8.5
Depth of Focus (mm)	15.8

The transducer was driven by bipolar signals generated and amplified by a trigger generator (AFG3252, Tektronix,

Beaverton, OR, USA). Ultrasound signals were acquired and digitized at a sampling frequency of 500 MHz. In practice, sampling rates between 3 and 10 times the center frequency are typically required. However, based on expert experience, 500 MHz is considered appropriate for use in self-built ultrasound systems [25], [26]. To convert each RF signal into ultrasound B-mode images while reducing spurious frequencies, a bandpass filter is installed before the signal is transmitted back to the A/D converter. Additionally, a series of processes including bandpass filtering, Hilbert transformation, logarithmic compression, and grayscale mapping were performed, with the dynamic range set to 42 dB. The developed imaging system achieved axial and lateral image resolutions of 140 and 190 μm, respectively, as measured with a 10-μm tungsten wire. Furthermore, each ultrasound image used as input to the proposed model corresponds to the class of workpiece porosity as the model output.

D. PROPOSED MCFNN FOR CLASSIFYING THE QUALITY OF METALLIC WORKPIECES FABRICATED VIA SLM

The proposed MCFNN model integrates the capability of CNNs to extract implicit knowledge from two-dimensional images with the advantage of FNNs; thus, the proposed model has high interpretability because of its human-like fuzzy inferencing ability. Furthermore, to improve the training efficiency, image classification performance, and interpretability of the proposed model, a multiscale mechanism inspired by CSPNet was included in it [27]. This mechanism enables the feature maps produced by the proposed model to preserve high-level information and these feature maps to be effectively reused across multiple scales of the network. The proposed MCFNN model comprises two parts: a feature extraction part with the image convolution operation (similar to the classical CNN) and a classification part with an FNN. The following text provides a detailed description of the multiscale mechanism and classification part.

1) CONCATENATION LAYER

In the concatenation layer of the proposed model, the previously used feature maps are concatenated to preserve the diversity and enrich their patterns. To concatenate them together, it is necessary for the feature map sizes to be the same. Therefore, two mechanisms were employed, such as zero padding and upsampling. The equation of this layer is expressed as follows:

$$y_n(x) = [f_1(x), \ldots, f_{n-1}(x), f_n(x)] \tag{2}$$

where [,] represents the concatenation operation and where $f_n(x)$ denotes the feature map calculated by the *nth* convolutional layer and pooling layer.

2) FUSION LAYER

Before inputting features into the FNN of the proposed model, a fusion layer is used as a transition layer to transform the features into one-dimensional information. Commonly used fusion strategies, as displayed in Fig. 5, include global average pooling (GAP) and channel average pooling (CAP). GAP was considered a suitable strategy for the proposed MCFNN due to its invariance to spatial variability and low sensitivity to noise in input images. The equation of this layer is expressed as follows:

$$GAP(i) = \frac{1}{h \times w} \sum_{h=1}^{h} \sum_{w=1}^{w} feature\_map(h, w, i) \tag{3}$$

where $GAP(i)$ is the output values for the ith channel after the GAP operations, and h and w are the spatial dimensions of the feature map.

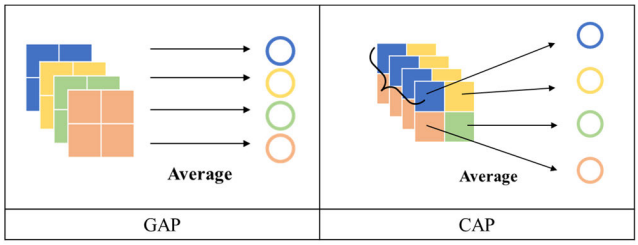

FIGURE 5. Fusion strategy of GAP and CAP.

3) LINGUISTIC TERM LAYER

In the linguistic term layer of the proposed model, each node implements a membership function, which is converted into a fuzzy value from a crisp input value through fuzzification. The Gaussian membership function is used in the proposed model; this function is expressed as follows:

$$o_{ij}^{L} = exp\left(-\frac{\left(o_i^F - m_{ij}\right)^2}{\left(\sigma_{ij}\right)^2}\right) \tag{4}$$

where o_{ij}^{L} is the output of the linguistic term layer and also represents the degree of Gaussian membership of the input value o_i^F, which is outputted from fusion layer. Additionally, m_{ij} and σ_{ij} denote the mean and standard deviation of the Gaussian function, respectively.

4) RULE LAYER

The rule layer of the proposed model establishes the connections between the term nodes and rule nodes used by the product operator; the equation of this layer is expressed as follows:

$$o_j^R = \prod_i^n o_{ij}^L \tag{5}$$

where o_j^R is the output of the rule layer.

5) DEFUZZIFICATION LAYER

The defuzzification layer of the proposed model mainly obtains the numerical outputs (y_j) of the defuzzification process. The weight w_{ij} represents the consequent fuzzy singleton between the *jth* rule node and the *ith* output node. The output of the aforementioned layer is obtained as follows:

$$o_j^D = \sum_{j=1}^{m} w_j o_j^R \tag{6}$$

$$y_j = \frac{o_j^D}{\sum_{j-1}^{m} o_j^R} \tag{7}$$

E. WORKPIECE QUALITY VERIFICATION

In subsection II-B, the measurement of porosity using Archimedes' principle is presented, and the classification task in this study is also based on the porosity of the workpieces. Yet, to verify the quality of the workpieces, third-party quality verification is necessary; therefore, the additional examination was performed using micro-CT scanning to measure the internal defect distributions of the metallic workpieces manufactured through SLM. Micro-CT scanning was conducted at the Metal Industries Research & Development Centre, Kaohsiung, Taiwan, by using an industrial scanner (Phoenix V|tome|x S240, Waygate Technologies, Hürth Germany).

III. EXPERIMENTAL RESULTS

This section describes in detail the experimental results, including the combinations of process parameters used in workpiece fabrication, the produced ultrasound B-mode images, the adopted concatenation methods, the adopted feature fusion strategies, the classification performance of the proposed MCFNN model and relevant state-of-the-art models, and micro-CT-based workpiece quality verification.

A. FABRICATION OF METALLIC WORKPIECES THROUGH SLM

A total of 24 metallic workpieces were manufactured through SLM under process parameter combinations selected according to the simulation results of a previous study. The energy density was set as approximately 165 or 82 J/mm^3; the laser power was set as 300 W; and the scanning speed was set as 850, 900, 950, or 1000 mm/s. The energy density ranged between 55.6 and 196.1 J/mm^3, and the layer thickness was 20 or 40 μm (Table 2). In general, the surface roughness of the workpieces with a layer thickness of 20 μm was lower than that of the workpieces with a layer thickness of 40 μm, possibly because the laser beam used to achieve a layer thickness of 20 μm had higher energy density than that used to achieve a layer thickness of 40 μm, which led to the Inconel powder being melted to a greater extent when the layer thickness was 20 μm. This phenomenon is illustrated in photographs of the workpieces captured using an optical camera (Fig. 6). Surface pores were observed on workpieces 17, 20, and 24.

TABLE 2. Process parameter combinations used in workpiece fabrication.

#	Energy density (J/mm^3)	#	Energy density (J/mm^3)
1	164.7 (P: 252 v: 850 t: 20)	13	82.4 (P: 252 v: 850 t: 40)
2	164.8 (P: 267 v: 900 t: 20)	14	82.4 (P: 267 v: 900 t: 40)
3	164.9 (P: 282 v: 950 t: 20)	15	82.5 (P: 282 v: 950 t: 40)
4	165.0 (P: 297 v: 1000 t: 20)	16	82.5 (P: 297 v: 1000 t: 40)
5	196.1 (P: 300 v: 850 t: 20)	17	98.0 (P: 300 v: 850 t: 40)
6	185.2 (P: 300 v: 900 t: 20)	18	92.6 (P: 300 v: 900 t: 40)
7	175.4 (P: 300 v: 950 t: 20)	19	87.7 (P: 300 v: 950 t: 40)
8	166.7 (P: 300 v: 1000 t: 20)	20	83.3 (P: 300 v: 1000 t: 40)
9	130.7 (P: 200 v: 850 t: 20)	21	65.4 (P: 200 v: 850 t: 40)
10	123.5 (P: 200 v: 900 t: 20)	22	61.7 (P: 200 v: 900 t: 40)
11	117.0 (P: 200 v: 950 t: 20)	23	58.5 (P: 200 v: 950 t: 40)
12	111.1 (P: 200 v: 1000 t: 20)	24	55.6 (P: 200 v: 1000 t: 40)

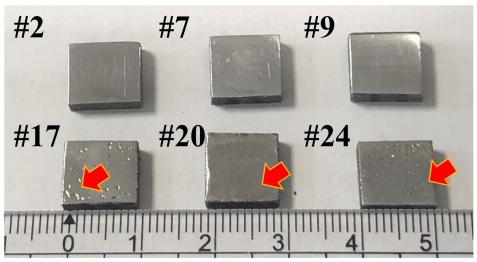

FIGURE 6. Photographs of some fabricated metallic workpieces.

B. ULTRASOUND IMAGE ACQUISITION

From subsection III-A, it can be deduced that workpieces with a layer thickness of 20 μm exhibit better quality due to the higher energy density. Consequently, to visualize the internal microstructure, ultrasound images of each workpiece were obtained using the high-frequency ultrasound system introduced in subsection II-C. In this regard, ultrasound images from six workpieces (#1, #2, #7, #17, #20, #24) with varying porosity levels, ranging from low to high, have been selected for presentation in Fig. 7. During UT, the workpieces were scanned for 15 mm in both the width and length directions by using a raster scanning strategy, and the x–y axial intervals were set as 40 μm. The water area in each ultrasound image was removed automatically using an algorithm designed to maintain the workpiece area. The workpieces with lower porosity (higher quality) exhibited a more homogeneous texture in the ultrasound B-mode images, indicating that more complex workpiece microstructures were associated with more lack-of-fusion defects and a lower energy density of the employed laser beam. Moreover, workpieces with higher porosity exhibited higher local signal intensity variation, which corresponded to a higher intensity of backscatterers in the ultrasound B-mode images. Furthermore, because of the propagation properties of ultrasound, linear patterns were exhibited by the workpieces, possibly resulting from the layer wise SLM manufacturing process, which introduced the horizontal variations observed in the ultrasound B-mode images.

C. WORKPIECE QUALITY CLASSIFICATION WITH THE MCFNN MODEL

This subsection provides details regarding the training, testing, and performance evaluations of the proposed MCFNN model. It also provides a comparison between the proposed

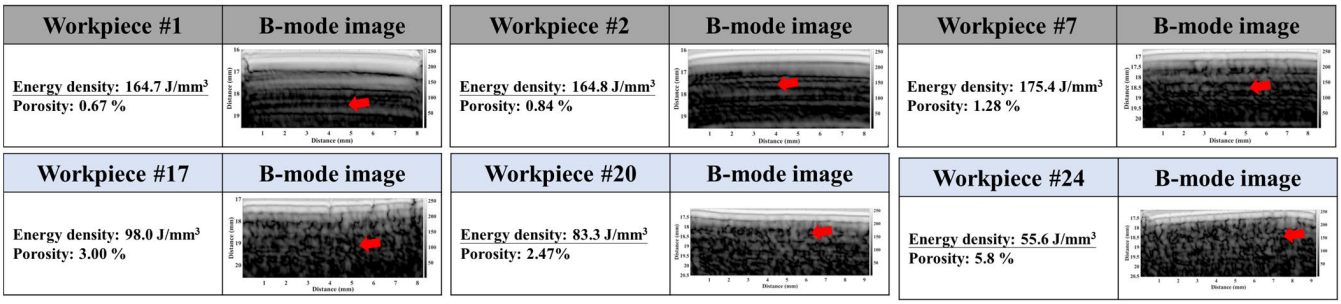

FIGURE 7. Ultrasound B-mode images obtained under various energy density and workpiece porosity values.

model and relevant state-of-the-art models. A total of 2700 ultrasound images were used for model training, and 900 ultrasound images were used for model testing. All the ultrasound images adopted for training and testing were resized to 128 × 128 pixels. A total of 20% of the training data was used as validation data. Specifically, to avoid misjudgments by the proposed model, the ultrasound B-mode images of one workpiece were assigned to only the training set or testing set and not to both of them. In the experimental environment, TensorFlow and Keras were used as the DL environment and development tool, respectively. The models examined in this study were trained on a 6-GB graphics processing unit (GeForce GTX 1060, NVIDIA, Santa Clara, California, USA) by using the Adagrad optimizer under a batch size of 8 for 20 epochs. Moreover, all the models were evaluated five times. The parameter settings of the MCFNN are presented in Table 3. To evaluate the performance of the examined models, the present study utilized five criteria: average accuracy, precision, recall, F1 score, and the number of training parameters. Specifically, the trainable parameters were acquired using the Python ''summary''' method.

TABLE 3. Parameter settings of the proposed MCFNN model.

Layer	Kernel size	Number of filters	Stride
Input	-	-	-
Convolution 1	3 × 3	32	1
Max pooling 1	2 × 2	-	2
Convolution 2	3 × 3	64	1
Max pooling 2	2 × 2	-	2
Convolution 3	3 × 3	128	1
Max pooling 3	2 × 2	-	2
Concatenate	[Max pooling 1, Max pooling 2, Max pooling 3]		
Fusion	-	128	-
Fuzzy rule	-	32	-
Defuzzification	-	Number of classes	-

1) CONCATENATION MECHANISM AND FUSION STRATEGIES COMPARISON

In the concatenation layer of the proposed model, each feature map should be expanded to a standard size. Two methods can be used to achieve this goal: zero padding and upsampling. Zero padding involves adding additional pixels around an image, and upsampling involves increasing the size of an image by using interpolation techniques. Tables 4 and 5 list the average accuracy, precision, recall, and F1 score of the MCFNN model when the zero-padding and upsampling concatenation methods were used with the GAP and CAP fusion strategies. Moreover, another type of fuzzy inference system, namely a TSK system (TSK-MCFNN) [28], was also considered in the present study. The experimental results obtained for the MCFNN, which included a multiscale fusion mechanism, were compared with those obtained for a convolutional FNN (CFNN) and a TSK-CFNN, both of which were designed without a multiscale fusion mechanism. The experimental results indicated that the MCFNN(GAP), MCFNN(CAP), TSK-MCFNN(GAP), and TSK-MCFNN(CAP) models, which used the upsampling method, exhibited the highest improvements in average accuracy, precision, recall, and F1 score (7.69 %, 8.15%, 7.69%, and 7.77%, respectively), compared to the models which used zero padding method. In general, GAP outperformed CAP in all the models on all the evaluation indices. Moreover, the multiscale mechanism enhanced model accuracy. For instance, the MCFNN(GAP) model had 3.31% higher accuracy than did the CFNN(GAP) model, and the TSK-MCFNN(GAP) model had 6.31% higher accuracy than did the TSK-CFNN(GAP) model that used the zero-padding method. Furthermore, the model with an FNN exhibited higher accuracy than did the TSK-based FNN model, possibly because the TSK-based FNN is less robust in the presence of noisy input data [29]. Overall, the proposed MCFNN(GAP) model exhibited the highest average accuracy, precision, recall, and F1 score when using the zero-padding and upsampling methods (90.02% and 91.44%, 91.24% and 92.74%, 90.02% and 91.44%, and 89.91% and 91.35%, respectively). In addition, the standard deviation of the proposed MCFNN was smaller than those of the other models.

TABLE 4. Performance of the MCFNN, CFNN, TSK-CFNN, and TSK-MCFNN models when using the zero-padding concatenation method with the GAP and CAP fusion strategies.

Evaluation matrix / Models	Accuracy (%)	Precision (%)	Recall (%)	F1 score (%)
CFNN(GAP)	86.71±10.64	89.76±7.31	86.71±10.64	86.14±11.44
CFNN(CAP)	82.09±7.31	85.50±6.16	82.09±7.31	81.55±7.63
TSK-CFNN(GAP)	83.64±6.53	85.21±6.76	83.64±6.53	83.46±6.57
TSK-CFNN (CAP)	76.53±9.83	79.09±11.48	76.53±9.83	76.17±9.7
MCFNN (GAP)	**90.02±6.55**	**91.24±5.84**	**90.02±6.55**	**89.91±6.66**
MCFNN (CAP)	86.84±6.92	88.69±6.4	86.84±6.92	86.65±7.03
TSK-MCFNN (GAP)	89.96±5.68	91.19±4.84	89.96±5.68	89.84±5.81
TSK-MCFNN (CAP)	77.51±9.65	80.17±10.94	77.51±9.65	77.11±9.62

TABLE 5. Performance of the MCFNN, CFNN, TSK-CFNN, and TSK-MCFNN models when using the upsampling concatenation method with the GAP and CAP fusion strategies.

Evaluation matrix / Models	Accuracy (%)	Precision (%)	Recall (%)	F1 score (%)
CFNN(GAP)	89.31±6.63	91.43±4.9	89.31±6.63	89.09±6.84
CFNN(CAP)	87.96±6.43	90.45±4.98	87.96±6.43	87.70±6.59
TSK-CFNN(GAP)	89.53±10.89	92.24±6.64	89.53±10.89	88.98±12.00
TSK-CFNN (CAP)	82.27±14.37	87.35±8.27	82.27±14.37	80.45±17.74
MCFNN (GAP)	**91.44±4.73**	**92.74±3.79**	**91.44±4.73**	**91.35±4.82**
MCFNN (CAP)	90.96±7.16	92.62±5.71	90.96±7.16	90.80±7.30
TSK-MCFNN (GAP)	90.42±5.85	91.43±5.32	90.42±5.85	90.34±5.91
TSK-MCFNN (CAP)	85.20±2.35	88.32±1.64	85.20±2.35	84.88±2.49

TABLE 6. Performance of the MCFNN model and the state-of-the-art models examined for comparison.

Evaluation matrix / Models	Accuracy (%)	Precision (%)	Recall (%)	F1 score (%)
Hu [30] / 2021	83.13±10.75	88.01±7.15	83.13±10.75	82.21±11.67
Kumaresan [31]/ 2023	82.71±11.31	88.03±7.19	82.71±11.31	81.64±12.46
Hua [32]/ 2022	89.98±8.70	92.22±6.58	89.98±8.70	89.72±8.95
Gong [33]/ 2020	88.31±9.64	90.57±7.50	88.31±9.64	87.98±10.04
Arbaoui [34]/ 2021	86.49±6.34	88.51±4.98	86.49±6.34	86.23±6.58
Medak [35]/2022	86.64±12.21	90.10±7.80	86.64±12.21	85.83±13.64
Bevan [36]/ 2022	86.98±4.86	88.60±4.13	86.98±4.86	86.81±4.98
MCFNN (GAP)	**91.44±4.73**	**92.74±3.79**	**91.44±4.73**	**91.35±4.82**

2) COMPARISON OF THE CLASSIFICATION PERFORMANCE OF THE PROPOSED MODEL AND RELEVANT STATE-OF-THE-ART MODELS

Since 2012, several major breakthroughs have been achieved in the performance and accuracy of deep NNs. Scholars have proposed models with deep or wide architectures to improve classification accuracy and those models have been used extensively as benchmarks in previous studies [30], [31], [32], [33], [34], [35], [36]. Therefore, in the present study, the classification performance of the MCFNN was

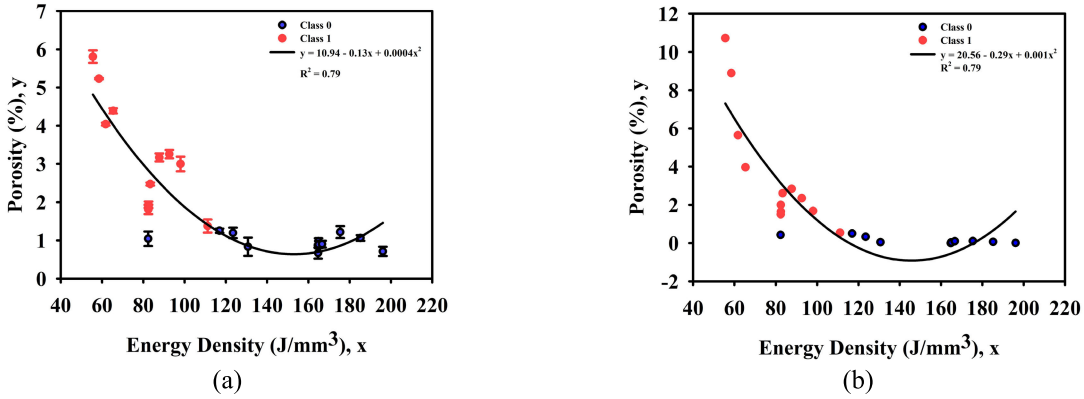

FIGURE 8. Variations in the porosity (a) calculated using Archimedes' principle and (b) measured through micro-CT scanning with the energy density.

compared with those of the aforementioned state-of-the-art models.

Table 6 presents the performance results of the proposed MCFNN model and the state-of-the-art models. The [32] and [33] models exhibited a higher accuracy and F1 score than did the other state-of-the-art models, possibly because those models utilize inception modules, which allow the network to choose from multiple convolutional filter sizes in each block. This concept is similar to the design concept of the proposed MCFNN. Overall, among all the compared models, the proposed MCFNN model exhibited the highest average accuracy, precision, recall, and F1 score (more than 90%) as well as the lowest standard deviations.

The proposed MCFNN model not only retained crucial features but also required fewer trainable parameters than did the other models. The proposed MCFNN required only 107,138 parameters, which was fewer than 5% of the number of trainable parameters required by [36].

D. MICRO-CT SCANNING VERIFICATION

The ground-truth data for the classification task were the porosity measurements conducted according to Archimedes' principle; therefore, the workpiece quality had to be verified through micro-CT scanning. The porosity measurement results are illustrated in Fig. 8. The porosity values calculated using Archimedes' principle and determined through micro-CT scanning exhibited similar variations in energy density, with the correlation coefficients being 0.79 in both cases. Specifically, the porosity of all the workpieces tended to decrease and then increase nonlinearly with an increase in the energy density, possibly because of the lack of fusion and keyhole pores caused by the utilized low and high LED [37].

IV. DISCUSSION

This section provides some valuable insights related to the results of this study regarding the selection of process parameters and the performance of the proposed MCFNN model.

A. FINDINGS REGARDING THE SELECTION OF PROCESS PARAMETERS

On the basis of a previous simulation study, the process map of Inconel 718 was divided into five parts to identify suitable process parameters for achieving optimal workpiece quality: areas with suitable substrate adhesion, extreme evaporation, keyhole melting, poor substrate adhesion, and an unstable single scan track. However, the suitable process parameters for only three areas (those with suitable substrate adhesion, extreme evaporation, and an unstable single scan track) were used in this study because workpieces constructed in the areas with keyhole melting and poor substrate adhesion had crucial defects that could have resulted in collisions between coating blade and workpieces [38]. Moreover, the experimental results indicated that the optimal process parameter combination was a laser power of 260 to 280 W and a scanning speed of 900 to 960 mm/s.

B. OBSERVATIONS RELATED TO THE PROPOSED MCFNN MODEL

The experimental results indicated that the models that used the upsampling concatenation method achieved higher accuracy than did those that used the zero-padding concatenation method. Both of these methods are applied to increase the spatial dimensions of feature maps; however, the upsampling method can enhance the extracted features to a greater extent than can the zero-padding method. Moreover, higher accuracy was achieved with the GAP fusion method than with the CAP fusion method, possibly because the channel-wise information of feature maps calculated from ultrasound B-mode images is less sensitive to image features. By contrast, GAP preserves the crucial characteristics of input images and thus improves model performance.

The defects caused discontinuous ultrasound signals due to the high surface roughness they induced. The state-of-the-art models couldn't correctly predict these images, possibly because ultrasound images have unique features and characteristics that differ from those of other medical images, such as magnetic resonance images or CT images. Consequently,

DL models might not be optimal for representing the features of ultrasound images. Overall, the results of this study indicate that the proposed MCFNN model is feasible for classifying the quality of metallic workpieces fabricated through SLM and that this model can learn robust representations from ultrasound images. Thus, improving the performance of this model through NDT appears worthwhile.

V. CONCLUSION

Quality assurance is an essential task for the production of high-quality metallic workpieces manufactured through AM, and this task requires the assessment of internal defects by using NDT techniques. In this study, an MCFNN model was designed to automatically evaluate the quality of workpieces fabricated through SLM from ultrasound B-mode images. Two concatenation methods (zero padding and upsampling), two feature fusion strategies (GAP and CAP), and the TSK fuzzy inference system were evaluated in this study. Moreover, the performance of state-of-the-art models was compared with that of the proposed MCFNN model. The proposed MCFNN model combines the multiscale feature extraction ability with the strengths of an FNN; thus, this model exhibits high accuracy in the classification of workpiece quality. The experimental results revealed that among the compared models, the MCFNN model that used the upsampling concatenation method and GAP feature fusion strategy achieved the highest average accuracy (91.44% $\pm$ 4.73%), precision (92.74% $\pm$ 3.79%), recall (91.44% $\pm$ 4.73%), and F1 score (91.35% $\pm$ 4.82%) for workpiece quality classification.

Overall, the proposed MCFNN demonstrated high accuracy with fewer trainable parameters, while UT has been proven as an effective and portable technique for detecting and evaluating surface, subsurface, and internal defects in tested objects. Therefore, integrating an automatic quality assessment system into a conventional UT system appears to be worthwhile and can yield economic benefits in the NDT field. Furthermore, the results of this study indicated that the developed MCFNN model has high potential for implementation in a UT system for industrial applications. However, it's worth noting that the input data of the proposed model only contains ultrasound images. Additional ultrasound parameters such as speed of sound, attenuation, and elasticity are valuable indicators that have not been considered in this study. To improve accuracy, future research will explore the deep investigation of extracting these features and combining them with images.

ACKNOWLEDGMENT

This work was financially supported by the "Intelligent Manufacturing Research Center" (iMRC) from The Featured Areas Research Center Program within the framework of the Higher Education Sprout Project by the Ministry of Education (MOE) in Taiwan.

REFERENCES

[1] A. Vafadar, F. Guzzomi, A. Rassau, and K. Hayward, "Advances in metal additive manufacturing: A review of common processes, industrial applications, and current challenges," *Appl. Sci.*, vol. 11, no. 3, p. 1213, Jan. 2021.

[2] C. Liu, L. L. Roux, Z. Ji, P. Kerfriden, F. Lacan, and S. Bigot, "Machine learning-enabled feedback loops for metal powder bed fusion additive manufacturing," *Proc. Comput. Sci.*, vol. 176, pp. 2586–2595, Jan. 2020.

[3] S. Hocine, H. Van Swygenhoven, and S. Van Petegem, "Verification of selective laser melting heat source models with *operando* X-ray diffraction data," *Additive Manuf.*, vol. 37, Jan. 2021, Art. no. 101747.

[4] W. Chen and Z. Li, "Additive manufacturing of titanium aluminides," in *Additive Manufacturing for the Aerospace Industry*, F. Froes and R. Boyer, Eds. Amsterdam, The Netherlands: Elsevier, 2019, pp. 235–263.

[5] P. Ninpetch, P. Kowitwarangkul, S. Mahathanabodee, P. Chalermkarnnon, and P. Rattanadecho, "Computational investigation of thermal behavior and molten metal flow with moving laser heat source for selective laser melting process," *Case Stud. Thermal Eng.*, vol. 24, Apr. 2021, Art. no. 100860.

[6] M. F. Sadali, M. Z. Hassan, F. Ahmad, H. Yahaya, and Z. A. Rasid, "Influence of selective laser melting scanning speed parameter on the surface morphology, surface roughness, and micropores for manufactured Ti6Al4V parts," *J. Mater. Res.*, vol. 35, no. 15, pp. 2025–2035, Aug. 2020.

[7] J. Liu, Y. Song, C. Chen, X. Wang, H. Li, C. Zhou, J. Wang, K. Guo, and J. Sun, "Effect of scanning speed on the microstructure and mechanical behavior of 316L stainless steel fabricated by selective laser melting," *Mater. Des.*, vol. 186, Jan. 2020, Art. no. 108355.

[8] Y. Kok, X. P. Tan, P. Wang, M. L. S. Nai, N. H. Loh, E. Liu, and S. B. Tor, "Anisotropy and heterogeneity of microstructure and mechanical properties in metal additive manufacturing: A critical review," *Mater. Des.*, vol. 139, pp. 565–586, Feb. 2018.

[9] M. Seifi, M. Gorelik, J. Waller, N. Hrabe, N. Shamsaei, S. Daniewicz, and J. J. Lewandowski, "Progress towards metal additive manufacturing standardization to support qualification and certification," *JOM*, vol. 69, no. 3, pp. 439–455, Mar. 2017.

[10] B. M. Colosimo, Q. Huang, T. Dasgupta, and F. Tsung, "Opportunities and challenges of quality engineering for additive manufacturing," *J. Quality Technol.*, vol. 50, no. 3, pp. 233–252, Jul. 2018.

[11] I. S. Ramírez, F. P. G. Márquez, and M. Papaelias, "Review on additive manufacturing and non-destructive testing," *J. Manuf. Syst.*, vol. 66, pp. 260–286, Feb. 2023.

[12] D. Cerniglia, M. Scafidi, A. Pantano, and J. Rudlin, "Inspection of additive-manufactured layered components," *Ultrasonics*, vol. 62, pp. 292–298, Jan. 2015.

[13] L. W. Koester, H. Taheri, T. A. Bigelow, P. C. Collins, and L. J. Bonds, "Nondestructive testing for metal parts fabricated using powder-based additive manufacturing," *Mater. Eval.*, vol. 76, no. 4, pp. 514–524, 2018.

[14] R. J. Smith, W. Li, J. Coulson, M. Clark, M. G. Somekh, and S. D. Sharples, "Spatially resolved acoustic spectroscopy for rapid imaging of material microstructure and grain orientation," *Meas. Sci. Technol.*, vol. 25, no. 5, May 2014, Art. no. 055902.

[15] C. Kim, H. Yin, A. Shmatok, B. C. Prorok, X. Lou, and K. H. Matlack, "Ultrasonic nondestructive evaluation of laser powder bed fusion 316L stainless steel," *Additive Manuf.*, vol. 38, Feb. 2021, Art. no. 101800.

[16] S. Yuan and X. Yu, "Ultrasonic non-destructive evaluation of selectively laser-sintered polymeric nanocomposites," *Polym. Test.*, vol. 90, Oct. 2020, Art. no. 106705.

[17] N. Huang, O. J. Cook, R. L. W. Smithson, C. M. Kube, A. P. Argüelles, and A. M. Beese, "Use of ultrasound to identify microstructure-property relationships in 316 stainless steel fabricated with binder jet additive manufacturing," *Additive Manuf.*, vol. 51, Mar. 2022, Art. no. 102591.

[18] Z. Xing, S. Zhao, W. Guo, F. Meng, X. Guo, S. Wang, and H. He, "Coal resources under carbon peak: Segmentation of massive laser point clouds for coal mining in underground dusty environments using integrated graph deep learning model," *Energy*, vol. 285, Dec. 2023, Art. no. 128771.

[19] P. V. de Campos Souza, "Fuzzy neural networks and neuro-fuzzy networks: A review the main techniques and applications used in the literature," *Appl. Soft Comput.*, vol. 92, Jul. 2020, Art. no. 106275.

[20] P. C. Souza, "Regularized fuzzy neural networks for pattern classification problems," *Int. J. Appl. Eng. Res.*, vol. 13, no. 5, pp. 2985–2991, 2018.

[21] G. Khodabandelou and M. M. Ebadzadeh, "Fuzzy neural network with support vector-based learning for classification and regression," *Soft Comput.*, vol. 23, no. 23, pp. 12153–12168, Dec. 2019.

[22] Z. Liu, X. Wang, H. Kim, Y. Zhou, W. Cong, and H. Zhang, "Investigations of energy density effects on forming accuracy and mechanical properties of Inconel 718 fabricated by LENS process," *Proc. Manuf.*, vol. 26, pp. 731–739, Jan. 2018.
[23] H.-C. Tran, Y.-L. Lo, T.-N. Le, A. K.-T. Lau, and H.-Y. Lin, "Multi-scale simulation approach for identifying optimal parameters for fabrication of high-density Inconel 718 parts using selective laser melting," *Rapid Prototyping J.*, vol. 28, no. 1, pp. 109–125, Jan. 2022.
[24] A. B. Spierings, M. Schneider, and R. Eggenberger, "Comparison of density measurement techniques for additive manufactured metallic parts," *Rapid Prototyping J.*, vol. 17, no. 5, pp. 380–386, Aug. 2011.
[25] M. M. Pasternak, A. Sadeghi-Naini, S. M. Ranieri, A. Giles, M. L. Oelze, M. C. Kolios, and G. J. Czarnota, "High-frequency ultrasound detection of cell death: Spectral differentiation of different forms of cell death in vitro," *Oncoscience*, vol. 3, nos. 9–10, pp. 275–287, Sep. 2016.
[26] C.-C. Huang and S.-H. Wang, "Blood coagulation and clot formation studies using high frequency ultrasounds," in *Proc. IEEE Ultrason. Symp.*, Montreal, QC, Canada, Mar. 2004, pp. 1757–1760.
[27] C.-Y. Wang, H.-Y. Mark Liao, Y.-H. Wu, P.-Y. Chen, J.-W. Hsieh, and I.-H. Yeh, "CSPNet: A new backbone that can enhance learning capability of CNN," in *Proc. IEEE/CVF Conf. Comput. Vis. Pattern Recognit. Workshops (CVPRW)*, Jun. 2020, pp. 1571–1580.
[28] T. Takagi and M. Sugeno, "Fuzzy identification of systems and its applications to modeling and control," *IEEE Trans. Syst., Man, Cybern.*, vol. SMC-15, no. 1, pp. 116–132, Jan. 1985.
[29] Y. Wang and Y. Chen, "A comparison of Mamdani and Sugeno fuzzy inference systems for traffic flow prediction," *Anbar J. Eng. Sci.*, vol. 9, no. 1, pp. 296–306, Jan. 2014.
[30] Y. Hu, Y. Lian, Y. Liu, Y. Jin, X. Hu, Z. Liu, Z. Lin, L. Li, G. He, and Y. Chu, "Ultrasound image preprocessing method for deep-learning-based fatty liver diagnosis," in *Advances in Graphic Communication, Printing and Packaging Technology and Materials*. Singapore: Springer, 2021, pp. 204–212.
[31] S. Kumaresan, K. S. J. Aultrin, S. S. Kumar, and M. D. Anand, "Deep learning-based weld defect classification using VGG16 transfer learning adaptive fine-tuning," *Int. J. Interact. Des. Manuf.*, vol. 2023, pp. 1–12, May 2023.
[32] C. Hua, S. Chen, G. Xu, Y. Lu, and B. Du, "Defect identification method of carbon fiber sucker rod based on GoogLeNet-based deep learning model and transfer learning," *Mater. Today Commun.*, vol. 33, Dec. 2022, Art. no. 104228.
[33] Y. Gong, J. Luo, H. Shao, K. He, and W. Zeng, "Automatic defect detection for small metal cylindrical shell using transfer learning and logistic regression," *J. Nondestruct. Eval.*, vol. 39, no. 1, p. 24, Mar. 2020.
[34] A. Arbaoui, A. Ouahabi, S. Jacques, and M. Hamiane, "Concrete cracks detection and monitoring using deep learning-based multiresolution analysis," *Electronics*, vol. 10, no. 15, p. 1772, Jul. 2021.
[35] D. Medak, L. Posilović, M. Subašić, M. Budimir, and S. Lončarić, "DefectDet: A deep learning architecture for detection of defects with extreme aspect ratios in ultrasonic images," *Neurocomputing*, vol. 473, pp. 107–115, Feb. 2022.
[36] R. L. T. Bevan and A. J. Croxford, "Automated detection and characterisation of defects from multiview ultrasonic imaging," *NDT & E Int.*, vol. 128, Jun. 2022, Art. no. 102628.
[37] S. J. Wolff, S. Lin, E. J. Faierson, W. K. Liu, G. J. Wagner, and J. Cao, "A framework to link localized cooling and properties of directed energy deposition (DED)-processed Ti-6Al-4 V," *Acta Mater.*, vol. 132, pp. 106–117, Jun. 2017.
[38] D. Bricín, M. Ackermann, Z. Jansa, D. Kubátová, A. Kříž, Z. Špirit, and J. Šafka, "Development of the structure of cemented carbides during their processing by SLM and HIP," *Metals*, vol. 10, no. 11, p. 1477, Nov. 2020.

CHUN-HUI LIN received the M.S. degree in computer science from The University of Texas at Dallas, TX, USA, in 2017. She is currently pursuing the Ph.D. degree in computer science and information engineering with National Cheng Kung University, Tainan, Taiwan. Her research interests include signal/image processing, ultrasound material characterization, non-destructive testing, intelligent control, and machine/deep learning.

CHENG-JIAN LIN (Senior Member, IEEE) received the B.S. degree in electrical engineering from the Ta Tung Institute of Technology, Taipei, Taiwan, in 1986, and the M.S. and Ph.D. degrees in electrical and control engineering from National Chiao-Tung University, Taiwan, in 1991 and 1996, respectively. Currently, he is a Chair Professor of the Computer Science and Information Engineering Department, National Chin-Yi University of Technology, Taichung, Taiwan, and the Dean of the Intelligence College, National Taichung University of Science and Technology, Taichung. His current research interests include machine learning, pattern recognition, intelligent control, image processing, intelligent manufacturing, and evolutionary robots.

SHYH-HAU WANG (Senior Member, IEEE) received the B.S. degree in biomedical engineering from Chung Yuan Christian University (CYCU), Chungli, Taiwan, in 1986, the M.S. degrees in biomedical engineering and in electrical engineering from Drexel University, Philadelphia, PA, USA, in 1992, and the Ph.D. degree in bioengineering from The Pennsylvania State University (PSU), University Park, PA, USA, in 1997.

He was a Research Associate with the Department of Biomedical Engineering, University of Virginia, in 1997, and then, he was a Postdoctoral Fellow with the NIH Ultrasound Transducer Resource Center, PSU, in 1998. Subsequently, he was with the Department of Biomedical Engineering, CYCU, as an Assistant Professor, in 1998, an Associate Professor, in 2001, and a Professor, in 2006. Since 2009, he has been with the Department of Computer Science and Information Engineering and the Institute of Medical Informatics, National Cheng Kung University, Tainan, Taiwan. His research interests include biomedical ultrasound imaging, ultrasound tissue/material characterization, signal/image processing, medical instrumentation and informatics, and machine/deep learning.